Alterations in the Local Myocardial Motion Pattern in Patients Suffering From Pressure Overload Due to Aortic Stenosis

M. Stuber, PhD; M.B. Scheidegger, PhD; S.E. Fischer, PhD; E. Nagel, MD; F. Steinemann, MD; O.M. Hess, MD; P. Boesiger, PhD

Background—MR tissue tagging allows the noninvasive assessment of the locally and temporally resolved motion pattern of the left ventricle. Alterations in cardiac torsion and diastolic relaxation of the left ventricle were studied in patients with aortic stenosis and were compared with those of healthy control subjects and championship rowers with physiological volume-overload hypertrophy.

Methods and Results—Twelve aortic stenosis patients, 11 healthy control subjects with normal left ventricular function, and 11 world-championship rowers were investigated for systolic and diastolic heart wall motion on a basal and an apical level of the myocardium. Systolic torsion and untwisting during diastole were examined by use of a novel tagging technique (CSPAMM) that provides access to systolic and diastolic motion data. In the healthy heart, the left ventricle performs a systolic wringing motion, with a counterclockwise rotation at the apex and a clockwise rotation at the base. Apical untwisting precedes diastolic filling. In the athlete's heart, torsion and untwisting remain unchanged compared with those of the control subjects. In aortic stenosis patients, torsion is significantly increased and diastolic apical untwisting is prolonged compared with those of control subjects or athletes.

Conclusions—Torsional behavior as observed in pressure- and volume-overloaded hearts is consistent with current theoretical findings. A delayed diastolic untwisting in the pressure-overloaded hearts of the patients may contribute to a tendency toward diastolic dysfunction. **(*Circulation*. 1999;100:361-368.)**

Key Words: magnetic resonance imaging ■ hypertrophy ■ stenosis ■ mechanics

Alterations in the local motion pattern of the myocardium have been described previously.[1–4] In pressure-overload hypertrophy, wall stress can be normal (adequate hypertrophy) or increased (inadequate hypertrophy).[5] The left ventricle (LV) responds to the pressure overload by developing LV hypertrophy, with addition of new sarcomeres in parallel to the existing ones. This results in an increase in wall thickness with little or no change in chamber radius.[6] Consequently, an increase in LV filling pressure with an upward shift of the diastolic pressure-volume relationship (diastolic dysfunction) occurs. In the heart that is pathologically hypertrophied as a result of aortic stenosis, a tendency toward diastolic dysfunction has already been reported.[7–9]

According to previously published results describing the mechanics that could generate torsion,[10] an increased torsional deformation is predicted in such pathologically hypertrophied hearts. In contrast, normal torsion is expected in volume-overloaded hearts with unchanged ratio of wall thickness to radius. The implications of LV hypertrophy and altered loading conditions on the regional wall motion and relaxation rate were investigated in aortic stenosis patients. For comparison purposes, championship rowers with physiological LV hypertrophy were examined as well. These 2 collectives were compared with control subjects (controls) with normal LV function.

Multiple imaging techniques for the assessment of regional wall motion exist.

One approach is the surgical implantation of tantalum markers into the myocardium.[11,12] In combination with x-ray angiography, the motion of these markers can then be recorded with high temporal and spatial resolution. With such an approach, torsional deformation of the heart can be recorded, and alterations in diastolic untwisting have been observed in heart transplant patients shortly before rejection.[2] Although this method is very powerful, it is invasive, requires ionizing radiation, and is inappropriate for clinical use. Alternative angiographic "markers," such as tracking of the bifurcations of the coronary arteries,[13] suffer from the limited number of landmarks and their irregular geometric distribution. Furthermore, they provide motion information only with

Received December 2, 1998; revision received April 27, 1999; accepted May 5, 1999.

From the Institute of Biomedical Engineering and Medical Informatics, University and ETH Zurich (M.S., M.B.S., S.E.F., P.B.), and the Department of Internal Medicine, Cardiology, University Hospital (E.N., F.S., O.M.H.), Zurich, Switzerland.

Correspondence to Prof Dr P. Boesiger, Institute of Biomedical Engineering and Medical Informatics, University and ETH Zurich, Gloriastrasse 35, CH-8092 Zurich, Switzerland. E-mail boesiger@biomed.ee.ethz.ch

***Circulation* is available at http://www.circulationaha.org**

TABLE 1. Patient Characteristics

Patients	n	Age, y	HR, bpm	LVSP, mm Hg	LVEDP, mm Hg	EF, %	ΔP, mm Hg	A_{AV}, cm^2
AS	12	58±13	74±10	211±29	21±6	66±6	63±11	0.8±0.2
PH	11	23±4	60±6	...	...	...	...	...
C	11	34±9	73±6	...	...	...	...	...

Number of measured individuals, age, and heart rate (HR). In AS patients, LV peak systolic pressure (LVSP), LV end-diastolic pressure (LVEDP), ejection fraction (EF), mean systolic pressure gradient at the aortic valve (ΔP), and the aortic valve area (A_{AV}) are listed for the AS patients. All the values given are means including 1 SD.

regard to epicardial layers of the myocardium. Alternative noninvasive methods, such as echocardiography or conventional MRI, do not allow for visualization of the exact local motion pattern of the myocardium because of the absence of structural reliably traceable landmarks. In 1988, Zerhouni et al[14] proposed a noninvasive MRI method (MR myocardial tagging) that locally saturates or labels the magnetization. The labels, which might be attached as lines or grids, are fixed with respect to the myocardial tissue and can be visualized for different cardiac phases. The method has been applied successfully and has been refined by several groups.[3,15–18] Because the tagging information decays under the influence of longitudinal relaxation of the magnetization, the fading of the tags restricts the application of these techniques to the systolic phase of the human cardiac cycle.

A further modification of the existing tagging techniques was proposed by Fischer et al[19] in 1993. This technique (complementary spatial modulation of magnetization, or CSPAMM) allows access to systolic as well as diastolic motion data, whereby the tagging contrast remains constant during the entire cardiac cycle.

If slices that are spatially fixed with respect to the scanner coordinate system are acquired, long-axis contraction during systole results in through-plane motion on short-axis images. This means that it is not always the same tissue elements that are imaged in the different heart phases and thus leads to interpretation errors and inaccurate results of the analysis. However, by the combination of CSPAMM with a slice-following imaging technique, the effects of through-plane motion can be suppressed.[20] Therefore, real 2D projections of the complex 3D motion pattern of any point on the myocardium can be traced reliably for the entire heartbeat cycle.

Methods

Study Population

A total of 34 subjects were included in the present analysis: 12 patients with pressure overload due to aortic stenosis (AS group), 11 healthy volunteers (C group), and 11 athletes of a world-championship rowing team with physiological hypertrophy (PH group) were investigated by use of CSPAMM myocardial tagging. Written informed consent was obtained from all participants, and the research protocol was approved by the hospital Committee on Clinical Investigation. Patients with aortic stenosis underwent cardiac catheterization for diagnostic purposes. In Table 1, the patient variables are summarized. Mean age, heart rate, LV systolic pressure, LV end-diastolic pressure, ejection fraction, mean systolic pressure gradient at the aortic valve, and aortic valve area are listed for the AS patients.

MR Examination Protocol

For the localization of the double-oblique imaging plane for the short-axis views of the myocardium, 2 scout scans are performed. The first transverse scout is followed by a single oblique scout in cine mode. On the end-diastolic image of the second scout, 2 double-oblique short-axis slices for the tagging examination of apex and base are defined. The apical imaging plane is positioned 1 cm above the apical endocardium, the basal plane 1 cm below the valvular plane. For motion tracking at these levels, a slice-following CSPAMM-based tagging pulse sequence[19,20] was implemented on a 1.5-T Gyroscan ACS II whole-body system (Philips Medical Systems). By this technique, a periodic sinusoidal modulation of the magnetization is attached to a thin slice of the myocardium (Figure 1, Tagging A) immediately after the detection of the R wave of the ECG. Subsequently, a thick slice encompassing the potential extent of motion of the selected thin slice is imaged periodically during the cardiac cycle (Figure 1, Imaging A). A multi–heart-phase gradient echo imaging sequence in partial echo mode with a short echo time of T_e=3.4 ms is used that strongly suppresses motion- or flow-induced artifacts. The same experiment is then performed a second time, whereby the modulation is inverted compared with the first experiment (Figure 1, Tagging B). Subsequent subtraction of the 2 temporally resolved data sets (Imaging A and Imaging B) results in signal components that exclusively contain information of the initially labeled thin slice. Signals of the surrounding tissue of the thick slice are suppressed by the subtraction procedure.[20]

Two sets of images with horizontally and vertically modulated stripe patterns, respectively, are acquired. By the multiplication of these 2 acquisitions, a grid pattern with 8-mm interstripe distance typically results, as documented in Figure 2. The time interval between the subsequently acquired 16 to 20 heart-phase images is 35 ms. The field of view is 360 mm, with an acquisition matrix of 256×256 data points and an in-plane resolution of 1.4×1.4 mm. The thickness of the tagged slice is 6 mm; the thickness of the imaged volume is related to the long-axis contraction and varies from 25 to 30 mm at the base and from 15 to 20 mm at the apex. Because of the location of the relevant tag information in a limited area of k space, a reduced k-space acquisition is applied with a scan percentage of 35%.[18,20] It considerably reduces overall measurement time but does not affect spatial resolution for motion detection. To obtain constant

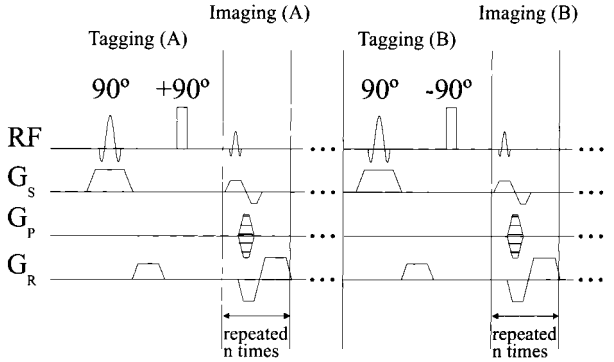

Figure 1. Pulse sequence for CSPAMM myocardial tagging. Before multi–heart-phase gradient echo imaging sequence (Imaging A), tagging pattern is attached to magnetization of selected slice (Tagging A). Entire sequence is applied twice, whereby sign of modulation function (Tagging B) of magnetization is inverted for every second acquisition (Imaging B).

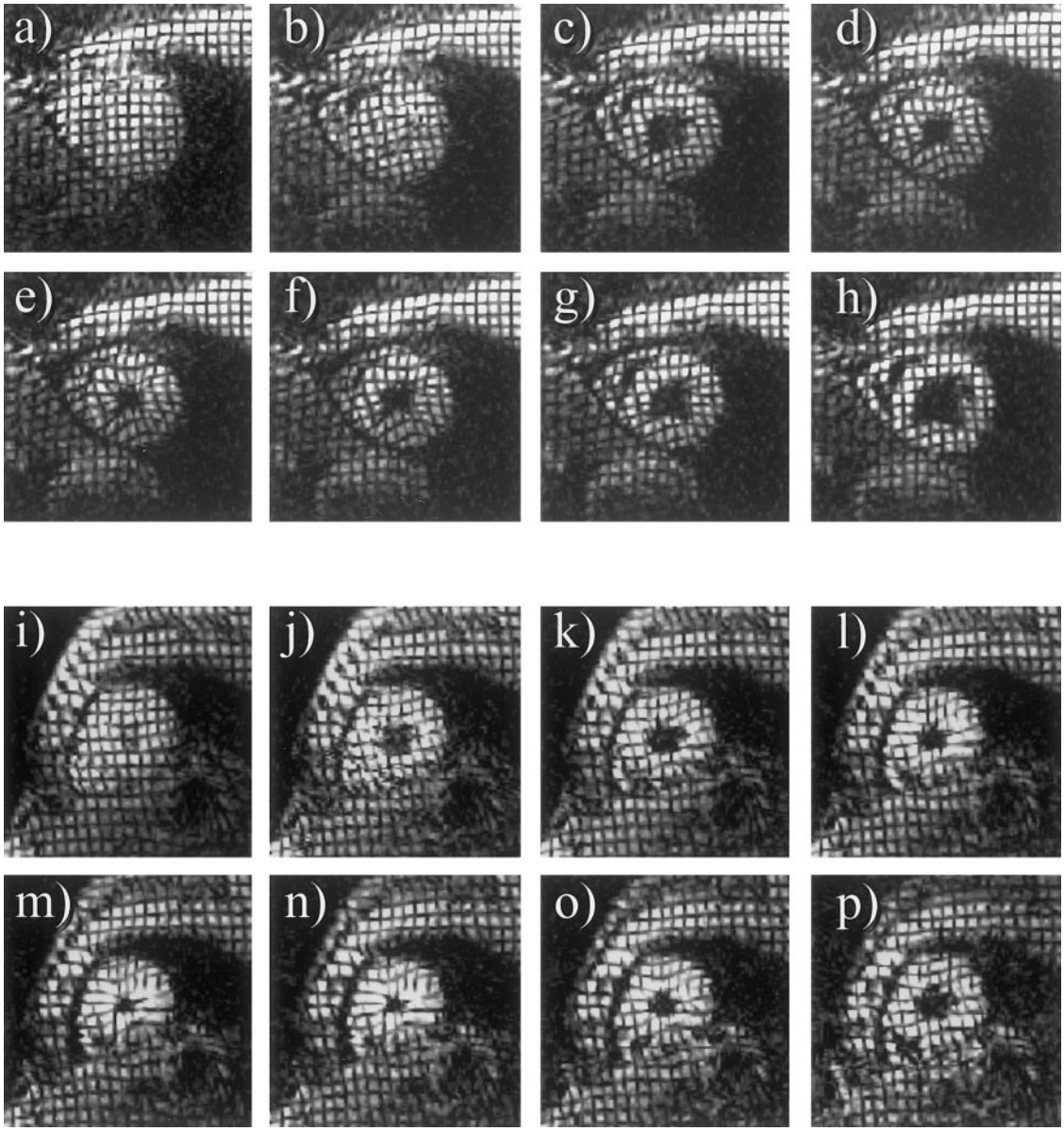

Figure 2. Representative apical images (n=8) in a healthy volunteer (top, a through h) and an AS patient (bottom, i through p). For both examples, every second acquisition out of a series of 16 images is shown. Temporal resolution for measured images is 35 ms, and spatial resolution is 1.4×1.4 mm.

tagging contrast for each heart phase, optimized radiofrequency-excitation angles are used (25° to 90°). Breathing-induced motion artifacts are reduced by a coached breathing pattern.[21] All patients and controls are investigated in the prone position with a cardiac surface coil (30-cm diameter) for signal acquisition.

Image Analysis

Individual end-diastolic long-axis length was measured in the images of the second scout scan. For the extraction of the tagged structures in the images, a user-assisted grid detection procedure[22] based on snake algorithms[23] is applied to each line-tagged time frame. With such sophisticated semiautomatic algorithms, the tags may be identified with subpixel resolution.[24] All evaluation steps for which user interaction is needed are performed on images that are zoomed by a factor of 6.

The next step of the procedure involves the definition of epicardial and endocardial contours of the LV by manual contouring. The center of gravity of the LV segment is used as a reference point. This allows for wall thickness measurements and the determination of the chamber radius, defined as the distance between the center of gravity and the midmyocardium. Fractional area change of the LV contour is also calculated. End systole is determined by the software by searching for the smallest inner cavity lumen in the time series of the images. To describe the local heart wall motion in a polar coordinate system, the 2 points at which the right ventricular endocardium merges with the LV epicardium are used as additional reference points. The interpolation of the original grid points by use of linear "shape functions" then allows for the characterization of the local heart wall motion in equidistant steps with respect to the circumference of the heart (Figures 3 and 4). Epicardial, endocardial, and midmyocardial points are calculated every 5° for each heart phase, resulting in 3×72 trajectories, which are partly visualized in Figures 3 and 4. The rotation of these points with respect to their initial position and to the center of gravity is then calculated by the software (Figure 5). Positive angle change or counterclockwise rotation is defined as viewed from the apex.[2] For all the measured collectives, average rotation of the 72 midmyocardial points are determined for the apical and basal levels of the heart. Torsion is defined to be

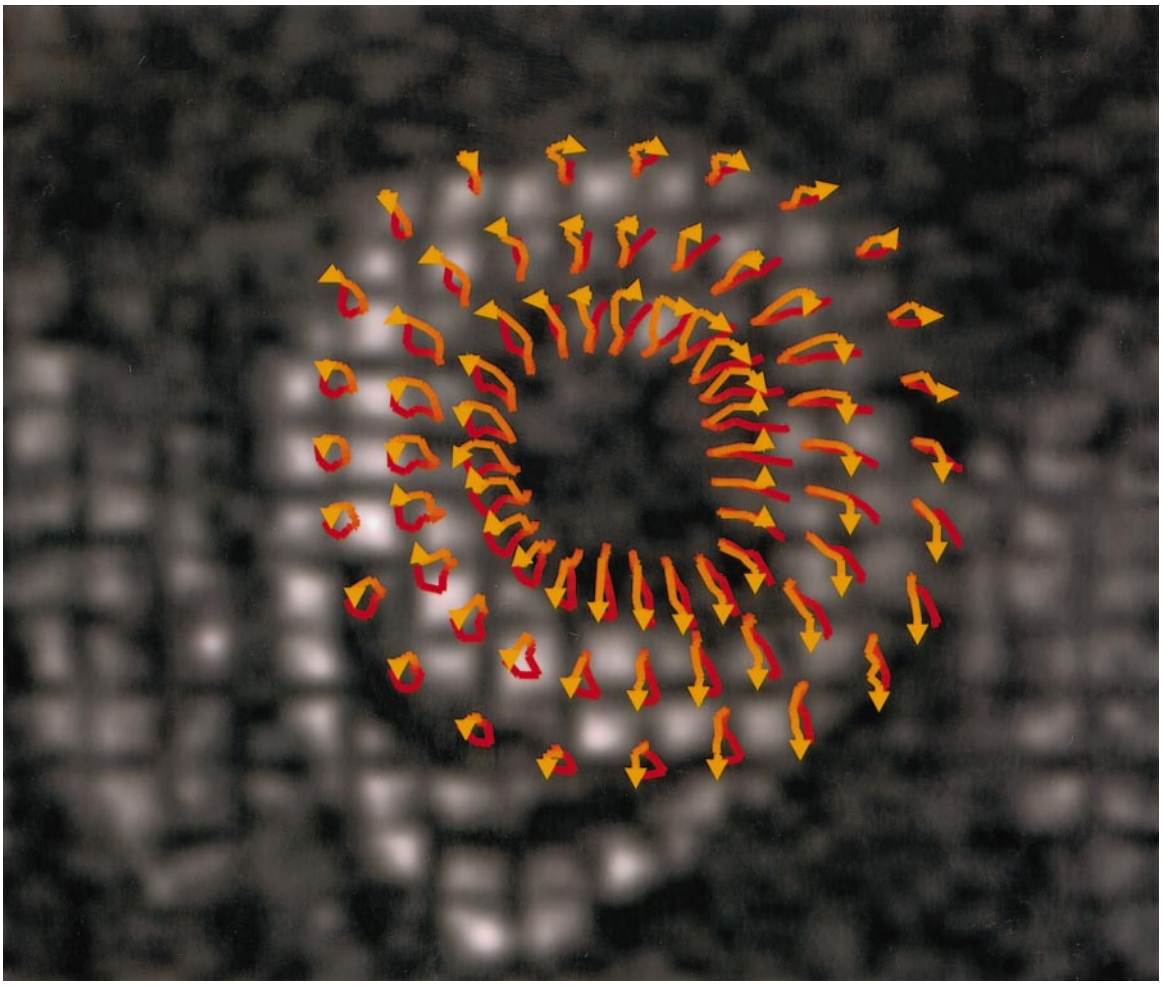

Figure 3. End-diastolic apical image in a healthy human. Tagged image is overlaid with corresponding local trajectories. Arrows start at beginning of systole (red) and end in late diastole (yellow). Regional differences are typical for healthy subjects as well as for AS patients.

proportional to the difference of averaged apical and basal rotation as measured in the midmyocardium. For normalization of torsion to heart size, torsion is measured as a function of end-diastolic base-to-apex distance.

Because isovolumic backrotation (untwisting) has been proved to be a sensitive parameter for the description of diastolic relaxation and filling,[17] rotation velocity and its peak value during diastolic untwisting is calculated as well. To account for individually dependent HRs, all the data are related to the duration of systole; ie, 100% on the time axis of Figure 6 refers to end systole. If measurements of time intervals are discussed, however, the values are provided in milliseconds as well.

Statistics

All values are given as mean±SD. Comparisons between the 3 groups (AS, PH, and C) are performed with Student's *t* test for unpaired comparisons. A value of $P<0.05$ is considered to be statistically significant.

Results

MR studies were completed in all subjects without complications. All the patients and volunteers were able to fulfill the requirements of the coached breathing pattern. In Tables 2 through 4, the parameters that are discussed in the following are summarized for AS, C, and PH.

Chamber Dimensions

End-diastolic ratio between apical wall thickness and chamber radius as measured on the end-diastolic MR images (first acquired heart-phase image after the detection of the R wave of the ECG) amounts to 0.84±0.1 in the patients (Table 2). This ratio differs significantly from the values found in the athletes (0.66±0.06; $P<0.01$) or the controls (0.65±0.07; $P<0.01$). If the same parameter is compared for athletes and controls, no significant difference can be reported ($P=0.7$). At the base, a similar tendency may be observed. The ratio of wall thickness to chamber radius amounts to 0.59±0.04 in the patients and to 0.50±0.09 in the athletes ($P=0.07$). In the controls, a value of 0.49±0.08 is found, which is slightly different from that in the patients ($P=0.1$) but the same as in the rowers ($P=0.9$).

If the end-diastolic wall areas at the apex are compared (Table 3), the AS patients and the rowers show a significantly increased muscle area (33±8 and 26±3 cm^2) compared with the controls (21±3 cm^2, $P<0.01$ and $P<0.01$). At the base, the AS patients and rowers show an increased muscle area (33±5 and 33±4 cm^2) compared with the controls (23±2 cm^2, $P<0.01$ and $P<0.01$). The athletes show a significantly enlarged lumen at the base (PH-C, $P<0.05$) and a moderately

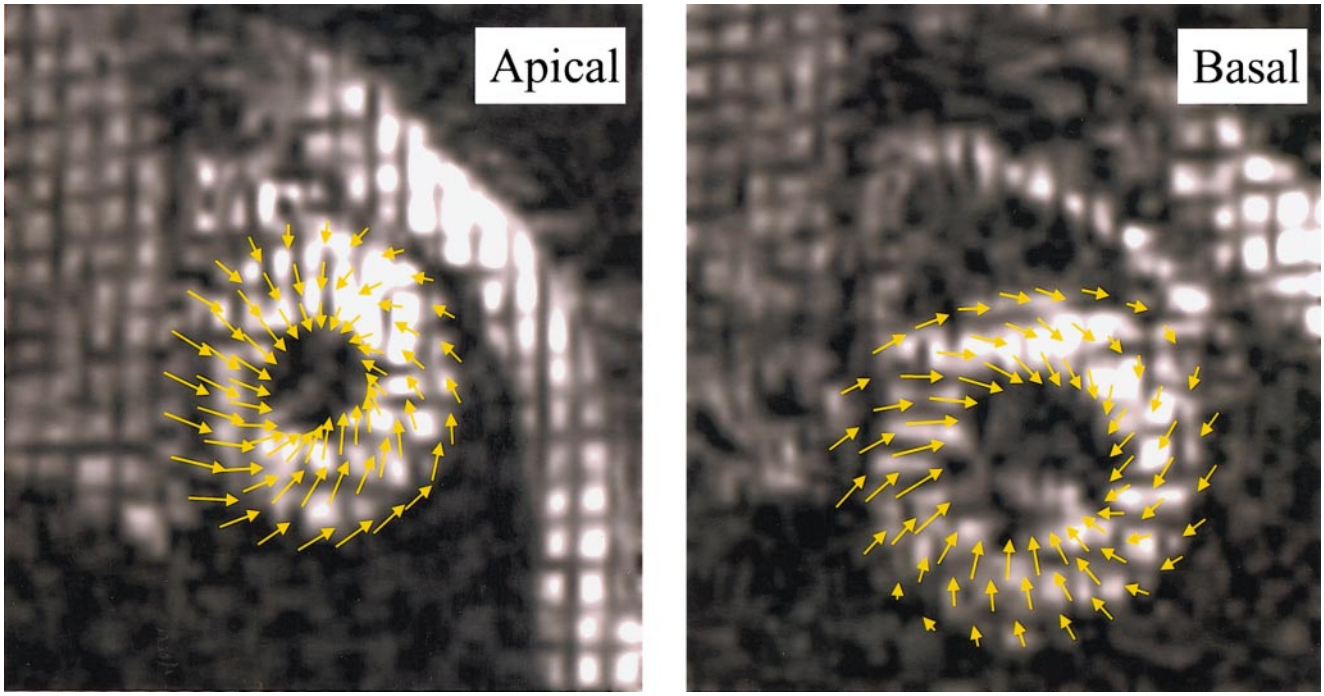

Figure 4. Ejection phase of LV at apex (left) and at base (right) of a healthy subject. End-systolic acquisitions are overlaid with corresponding local trajectories. At apex, contraction is associated with a counterclockwise rotation (as viewed from apex), whereas at base, a clockwise rotation is observed.

enlarged lumen at the apex. Compared with the controls, the AS patients show a highly significant increased wall area at both levels of the heart. If the lumina of apex and base are compared for these 2 groups, the AS patients show no significant chamber enlargement. If the rowers are compared with the healthy subjects, an increased cross-sectional muscle mass can be reported at apex and base of the athletes.

Torsional Deformation of the Heart

During systole, a clockwise rotation at the base is observed as viewed from the apex. Thus, ejection is supported by a torsional deformation of the heart (Figure 6A), with a counterclockwise rotation at the apex and a clockwise rotation at the base.[1–3,11,17] End-systolic torsion in the controls was 0.6±0.1°/cm when normalized to the long-axis length (Table 3). During systole, a counterclockwise apical rotation (positive angle change) as viewed from the apex can be observed in the healthy heart. Maximum rotation at the apex was 6.8±2.0° in the control group (Figure 6B). During isovolumic relaxation, a rapid clockwise untwisting with a peak untwisting velocity of 54.8±16.5°/s is observed at the apex (Table 4). Diastolic relaxation time, $T_{untwist}$ (time delay between end systole and maximum untwisting velocity) (Figure 6C, Table 4) was 46.6±23.0 ms in controls, or 16±7.6% in relation to the duration of systole.[2] Analogous to conventional pressure-volume loops, Figure 7 shows an apical rotation-area loop of 1 cardiac cycle. The loop is oriented clockwise and starts with the contraction of the LV. In controls, contraction and rotation occur almost simultaneously (Figure 7, 1). After the ejection phase, a fast backrotation in the direction opposite the systolic rotation can be observed (Figure 7, 2). During this period, almost no changes in cavity lumen are detected (isovolumic relaxation). In the subsequent filling phase (Figure 7, 3), no major rotational component can be seen. This means that there is a distinct separation between untwisting and filling in the healthy heart.

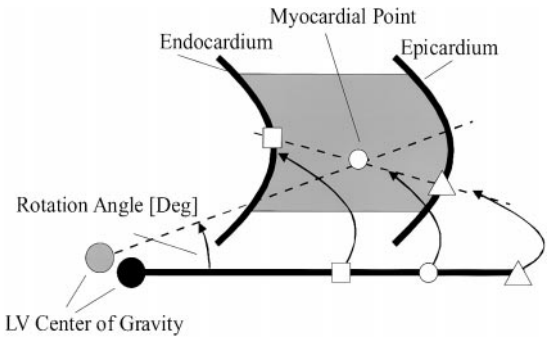

Figure 5. Quantification of local rotation angles of epicardial, endocardial, and midmyocardial regions. Angle is defined by position of a specific tissue element at 2 different time points, and center of gravity by endocardial and epicardial borders, respectively, of corresponding cardiac phase.

In the athletes, end-systolic torsion was 0.7±0.1°/cm (Table 3), which does not differ significantly from the value seen in the controls (P=0.58).

Maximum rotation at the apex was 5.7±1.8° in rowers (P=NS versus controls). Maximum untwisting velocity was 55.9±7.8°/s (Table 4), identical to that of the controls (P=0.9). The time interval between the time point of the smallest lumen and maximum backrotation velocity ($T_{untwist}$) was 50.7±23.3 ms (16.9±7.7% in percent of end systole). This time interval was identical for rowers and controls (P=NS). In the rotation-area loop of Figure 7, a distinct

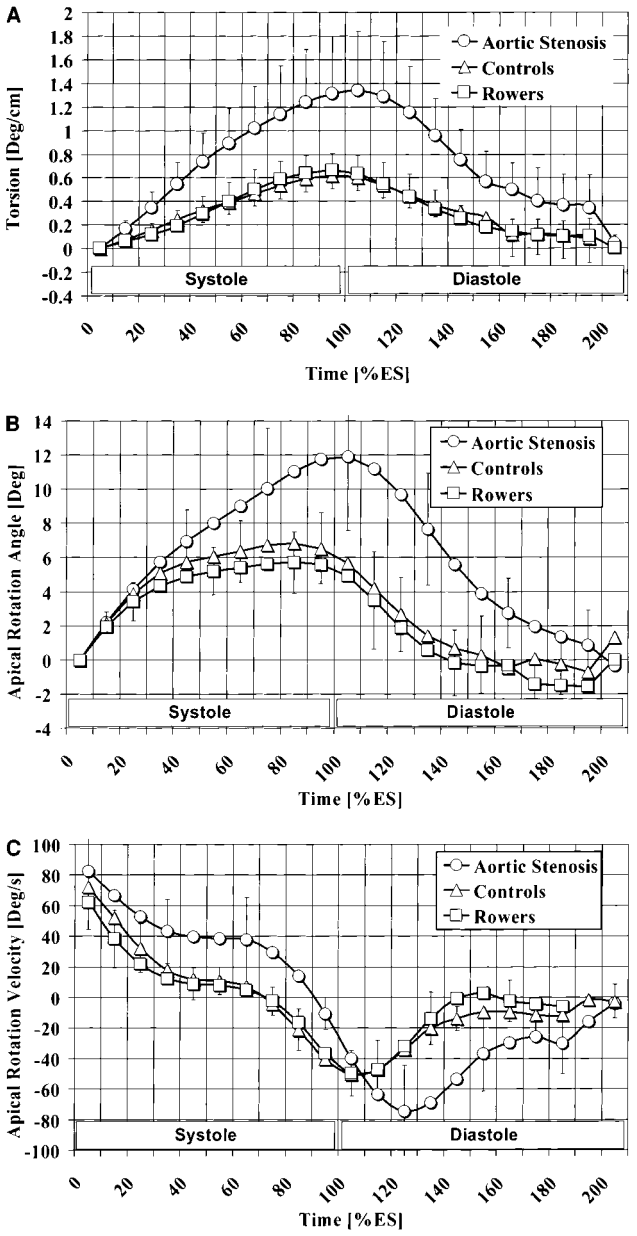

Figure 6. A, Mean torsional deformation (normalized to long-axis length) of LV (degrees/cm) including 1 SD in AS patients, controls, and rowers during 1 cardiac cycle. Torsion is plotted as a function of time normalized to end systole (=100%). B, Mean apical rotation angle (degrees) including 1 SD in AS patients, controls, and rowers during 1 cardiac cycle. Rotation angles are plotted as a function of time normalized to end systole (=100%). C, Mean apical rotation velocity (degrees/s) including 1 SD in AS patients, controls, and rowers normalized to end systole. Values above *x* axis (rotation velocity >0°/s) indicate counterclockwise rotation, whereas values below *x* axis refer to clockwise rotation as viewed from apex.

separation of untwisting and filling can be observed in the rowers. Again, apical untwisting in the rower's heart occurs mainly during isovolumic relaxation.

In the AS patients, a systolic torsion of 1.4±0.5°/cm is observed (Table 3). This value is significantly increased ($P<0.05$ versus controls and athletes).

Maximum apical twist amounts to 12.3±4.7° in patients with aortic stenosis. This significantly exceeds the values

TABLE 2. MR Data 1

	Wall Thickness/Radius	
Patients	Apical	Basal
AS	0.84±0.10	0.59±0.04
C	0.65±0.07	0.49±0.08
PH	0.66±0.06	0.50±0.09

Ratio of end-diastolic wall thickness to radius as measured on the first acquired image (35 ms after the detection of the R wave of the ECG). These values are given for the base and apex. All the values given are means including 1 SD.

seen in the volunteers (6.8±1.0°, $P<0.01$) or athletes (5.7±1.8°, $P<0.01$). In all the patients, maximum apical untwisting velocity (Table 4) is increased with respect to controls (80.0±28.8°/s versus 54.8±16.5°/s, $P<0.08$) or athletes (55.9±7.8°/s, $P<0.08$). The apical untwisting time in AS patients is 88.43±19.3 ms (32.4±6.3%) and is prolonged not only for the absolute value ($P<0.01$) but also when normalized to the duration of systole ($P<0.001$). AS patients also show a delayed apical untwisting with respect to the rowers ($P<0.05$; $P<0.001$ for percent changes). The rotation-area loop in Figure 7 clarifies the differences of the apical untwisting/relaxation pattern found in the patients. During diastole, untwisting and filling of the LV occur almost simultaneously. This suggests that there is a less distinct separation of untwisting and filling than seen in the normal heart.

Discussion

In the healthy heart, the basoapical torsional deformation is built up during systole (systolic wringing motion). During isovolumic relaxation, a rapid apical clockwise untwisting that precedes diastolic filling of the LV can be reported.[17] Apical backrotation and ventricular filling are temporally separated. In the physiologically hypertrophied heart, exactly the same motion pattern as in the volunteers was found. The data do not suggest any difference in torsion, apical peak rotation, or untwisting time, despite the increased size of the athlete's heart.

Pressure-overload hypertrophy is associated with a significantly increased systolic torsional deformation of the LV. This increased torsional deformation is accompanied by an increase in apical rotation. Systolic torsion tends to equalize sarcomere shortening between endocardial and epicardial layers of the LV.[10] Without torsional deformation of the heart, substantial transmural inhomogeneities of sarcomere shortening may be expected. Thus, with an increased wall thickness (in relation to the chamber radius), such inhomogeneities would be increased. According to this hypothesis, no increased torsional deformation is expected in volume-overload hearts in which the ratio of thickness to radius is maintained. This may be supported by the present findings in the athletes (with nonincreased ratio of wall thickness to chamber radius), in whom no increase in torsional deformation of the heart was found. In contrast, the hypothesis also predicts an increased torsion in the presence of an increased ratio of thickness to radius. This can also be confirmed by the present torsion data found in the pressure-overloaded hearts.

TABLE 3. MR Data 2

Patients	Torsion, °	$L_{long\ axis}$, cm	$Torsion_N$, °/cm	Wall Area, Apex, cm^2	Wall Area, Base, cm^2	Cavity Area, Apex, cm^2	Cavity Area, Base, cm^2
AS	14±5	10±1	1.4±0.5	33±8	33±5	7±3	14±3
C	6±1	10±1	0.6±0.1	21±3	23±2	8±2	14±3
PH	8±2	12±1	0.7±0.1	26±3	33±4	9±2	19±4

Systolic torsion, long-axis length ($L_{long\ axis}$), and torsion normalized to the long-axis length ($Torsion_N$). Wall area and volume of the lumen are indicated for end diastole as determined on the images acquired 35 ms after the detection of the R wave of the ECG. These values are given for the base and the apex. All the values given are means including 1 SD.

TABLE 4. MR Data 3

			$T_{untwist}$	
Patients	Rotation, °	ω_{max}, °/s	ms	×100% ES
AS	12±5	80±29	88±19	32±6
C	7±2	55±17	47±23	16±8
PH	6±2	56±8	51±23	17±8

Apical systolic peak rotation, peak diastolic untwisting velocity at the apex (ω_{max}), and relaxation time ($T_{untwist}$) (ms) and in percent of end systole (×100% ES). Untwisting time is defined as time delay between time of minimum inner cavity area and peak untwisting velocity. All the given values are means including 1 SD.

The potentially rearranged fiber architecture in the AS patients[7] may support the alterations in the torsional deformation of the heart.[25]

Most obviously, the amount of systolic apical twist needs to be compensated by a diastolic backrotation, or untwisting. In AS patients, apical peak rotation is significantly increased. Thus, during diastole, an increase in untwisting velocity or a prolongation of untwisting is expected. In the pressure-overloaded hearts due to aortic stenosis, a tendency toward an increased untwisting velocity and a significant prolongation of untwisting duration into the filling phase of the LV is seen. Because of the prolongation of apical diastolic untwisting, there is an overlap of untwisting and filling. Apical systolic rotation behavior basically restates the findings for torsion. Moreover, untwisting at the apex may also be used for the characterization of diastolic properties of the LV. Thus, apical rotational mechanics may be important but remain to be further investigated.

CSPAMM MR myocardial tagging has potential for noninvasive study of regional cardiac motion of the LV with high spatial and temporal resolution. A temporal resolution of 35 ms allows assessment of rapid cardiac motion components, such as diastolic untwisting. By the application of a sophisticated MR tagging procedure, the fading of the tags is suppressed, and thus, systolic as well as diastolic motion becomes accessible within 1 single imaging procedure. In addition, by the application of a slice-following procedure, the disadvantageous effects of through-plane motion may be avoided. As a consequence, motion of the same tissue elements can be traced throughout the entire cardiac cycle. A further enhancement of the technique toward clinical applicability may be expected if the method is combined with respiratory gating or navigator-controlled techniques.[26]

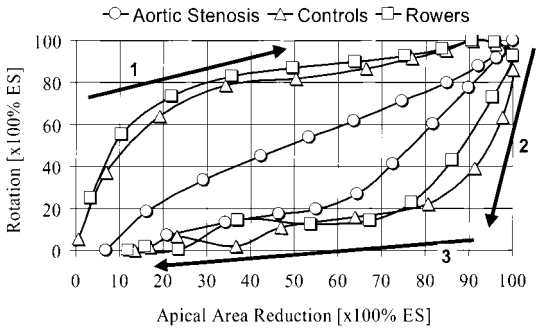

Figure 7. LV rotation-area loop (apical plane) in controls, rowers, and patients with aortic stenosis. Loop is separated into 3 phases: ejection (1), isovolumic relaxation (2), and filling (3) of LV.

Conclusions

The predicted systolic torsional behavior of hypertrophied hearts (both pathological and physiological) could be successfully verified in the present study. In terms of torsion or apical untwisting, a volume-overloaded heart does not differ from the heart of a healthy subject without volume overload. In the AS patients investigated, a delayed apical untwisting during diastole may contribute to a potential diastolic dysfunction.

Acknowledgments

This research project was financially supported by EUREKA and the Swiss Commission for Technology and Innovation. The authors also thank Philips Medical Systems, Best, Netherlands, for technical and financial support. The authors thank E.M. Pedersen, Skejby University Hospital, Aarhus, Denmark, and Christian Matter, Brigham and Women's Hospital, Boston, Mass, for helpful discussions.

References

1. Hansen DE, Daughters GT II, Alderman EL, Stinson EB, Baldwin JC, Miller DC. Effect of acute human cardiac allograft rejection on left ventricular systolic torsion and diastolic recoil measured by intramyocardial markers. *Circulation*. 1987;76:998–1008.
2. Yun KL, Niczyporuk MA, Daughters GT II, Ingels NB Jr, Stinson EB, Alderman EL, Hansen DE, Miller DC. Alterations in left ventricular diastolic twist mechanics during acute human cardiac allograft rejection. *Circulation*. 1991;83:962–973.
3. Maier SE, Fischer SE, McKinnon GC, Hess OM, Krayenbuehl HP, Boesiger P. Evaluation of left ventricular segmental wall motion in hypertrophic cardiomyopathy with myocardial tagging. *Circulation*. 1992;86:1919–1928.
4. Matheijssen NA, de Roos A, Doornbos J, Reiber JH, Waldman GJ, van der Wall EE. Left ventricular wall motion analysis in patients with acute myocardial infarction using magnetic resonance imaging. *Magn Reson Imaging*. 1993;11:485–492.
5. Julius BK, Spillmann M, Vassalli G, Villari B, Eberli FR, Hess OM. Angina pectoris in patients with aortic stenosis and normal coronary arteries: mechanisms and pathophysiological concepts. *Circulation*. 1997; 95:892–898.
6. Grossman W, Jones D, McLaurin LP. Wall stress and patterns of hypertrophy in the human left ventricle. *J Clin Invest*. 1975;56:56–64.

7. Hess OM, Schneider J, Koch R, Bamert C, Grimm J, Krayenbuehl HP. Diastolic function and myocardial structure in patients with myocardial hypertrophy: special reference to normalized viscoelastic data. *Circulation*. 1981;63:360–371.
8. Hess OM, Lavelle JF, Sasayama S, Kemper WS, Ross J. Diastolic myocardial wall stiffness of the left ventricle in chronic pressure overload. *Eur Heart J*. 1982;3:315–324.
9. Hess OM, Villari B, Krayenbuehl HP. Diastolic dysfunction in aortic stenosis. *Circulation*. 1993;87(suppl IV):IV-73–IV-76.
10. Arts T, Reneman RS. Dynamics of left ventricular wall and mitral valve mechanics: a model study. *J Biomech*. 1989;22:261–271.
11. Ingels NB Jr, Daughters GT II, Stinson EB, Alderman EL. Measurement of midwall myocardial dynamics in intact man by radiography of surgically implanted markers. *Circulation*. 1975;52:859–867.
12. McDonald IG. The shape and movements of the human left ventricle during systole: a study by cineangiography and by cineradiography of epicardial markers. *Am J Cardiol*. 1970;26:221–230.
13. Potel MJ, Rubin JM, MacKay SA, Aisen AM, Al-Sadir J, Sayre RE. Methods for evaluating cardiac wall motion in three dimensions using bifurcation points of the coronary arterial tree. *Invest Radiol*. 1983;18:47–57.
14. Zerhouni EA, Parish DM, Rogers WJ, Yang A, Shapiro EP. Human heart: tagging with MR imaging: a method for noninvasive assessment of myocardial motion. *Radiology*. 1988;169:59–63.
15. Axel L, Dougherty L. MR imaging of motion with spatial modulation of magnetization. *Radiology*. 1989;171:841–845.
16. Bolster BD Jr, McVeigh ER, Zerhouni EA. Myocardial tagging in polar coordinates with use of striped tags. *Radiology*. 1990;177:769–772.
17. Rademakers FE, Buchalter MB, Rogers WJ, Zerhouni EA, Weisfeldt ML, Weiss JL, Shapiro EP. Dissociation between left ventricular untwisting and filling: accentuation by catecholamines. *Circulation*. 1992;85:1572–1581.
18. McVeigh ER, Atalar E. Cardiac tagging with breath-hold cine MRI. *Magn Reson Med*. 1992;28:318–327.
19. Fischer SE, McKinnon GC, Maier SE, Boesiger P. Improved myocardial tagging contrast. *Magn Reson Med*. 1993;30:191–200.
20. Fischer SE, McKinnon GC, Scheidegger MB, Prins W, Meier D, Boesiger P. True myocardial motion tracking. *Magn Reson Med*. 1994;31:401–413.
21. Doyle M, Scheidegger MB, de Graaf RG, Vermeulen J, Pohost GM. Coronary artery imaging in multiple 1-sec breath holds. *Magn Reson Imaging*. 1993;11:3–6.
22. Stuber M, Nagel E, Fischer SE, Spiegel MA, Scheidegger MB, Boesiger P. Quantification of the local heartwall motion by magnetic resonance myocardial tagging. *Comput Med Imaging Graph*. 1998;22:217–228.
23. Kumar S, Goldgof D. Automatic tracking of SPAMM grid and the estimation of deformation parameters from cardiac MR images. *IEEE Trans Med Imaging*. 1994;13:122–132.
24. Atalar E, McVeigh ER. Optimization of tag thickness for measuring position with magnetic resonance imaging. *IEEE*. 1994;13:152–160.
25. Carew TE, Covell JW. Fiber orientation in hypertrophied canine left ventricle. *Am J Physiol*. 1979;236:H487–H493.
26. Chuang ML, Chen MH, Khasgiwala VC, McConnell MV, Edelman RR, Manning WJ. Adaptive correction of imaging plane position in segmented k-space cine cardiac MRI. *J Magn Reson Imaging*. 1997;7:811–814.

Alterations in the Local Myocardial Motion Pattern in Patients Suffering From Pressure Overload Due to Aortic Stenosis

M. Stuber, M. B. Scheidegger, S. E. Fischer, E. Nagel, F. Steinemann, O. M. Hess and P. Boesiger

Circulation. 1999;100:361-368
doi: 10.1161/01.CIR.100.4.361
Circulation is published by the American Heart Association, 7272 Greenville Avenue, Dallas, TX 75231

Print ISSN: 0009-7322. Online ISSN: 1524-4539